

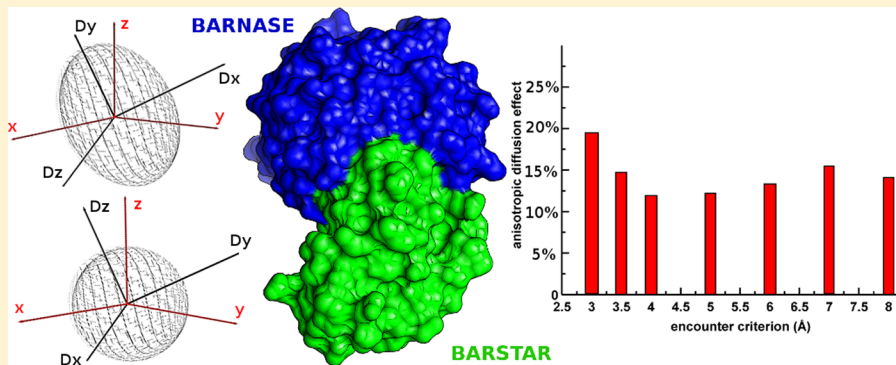
Anisotropic Diffusion Effects on the Barnase–Barstar Encounter Kinetics

Maciej Długosz*,† and Jan M. Antosiewicz‡

†Centre of New Technologies, University of Warsaw, Żwirki i Wigury 93, Warsaw 02-089, Poland

‡Department of Biophysics, Faculty of Physics, University of Warsaw, Żwirki i Wigury 93, Warsaw 02-089, Poland

Supporting Information



ABSTRACT: We investigated effects of hydrodynamic anisotropy on the kinetics of a diffusional encounter of a bacterial ribonuclease, barnase, and its natural inhibitor barstar, using the rigid-body Brownian dynamics technique. We performed atomistically detailed Brownian dynamics simulations of barnase and barstar under periodic boundary conditions, taking into account excluded volume and electrostatic and hydrophobic interactions between the proteins. We studied their specific (i.e., orientationally restricted by their configuration in the X-ray complex) and nonspecific association, either taking into account hydrodynamic anisotropy of the proteins or treating them as hydrodynamically equivalent spheres. We found that even relatively small anisotropy of associating proteins may influence the rate of their encounter and this effect is quantitatively measurable in the simulations. The role of the anisotropic diffusion manifests itself only in case of specific encounters while the association toward nonspecific complexes is not influenced by anisotropic diffusion. Association rate constants obtained from Brownian dynamics simulations for the studied system are up to 20% larger when hydrodynamic anisotropies of barnase and barstar are taken into account. Moreover, the dissociation from the specific complex is also accelerated in case of anisotropic diffusion.

1. INTRODUCTION

In dilute solutions, diffusional properties of molecules are determined by their size and shape, as well as by the temperature and viscosity of the solvent. The information required to characterize translational and rotational movements of quasi-rigid Brownian particles in dilute solutions is contained in their diffusion tensors. Single-particle diffusion tensor, D , is represented by a symmetric, 6×6 matrix containing four 3×3 blocks related to the translational (tt) and rotational diffusivities (rr) and their couplings (rt, tr):¹

$$D = \begin{pmatrix} D^{tt} & D^{tr} \\ D^{rt} & D^{rr} \end{pmatrix} \quad (1)$$

Diffusion tensors of molecules can be obtained theoretically from rigid-body hydrodynamic calculations performed for atomistically detailed molecular models.^{2–4} For a spherical particle the above matrix takes the diagonal form (isotropic diffusion) in which identical elements D_{ii}^{tt} correspond to the translational diffusion coefficient of a sphere. Similarly, identical

elements D_{ii}^{rr} give its rotational diffusion coefficient. For an arbitrarily shaped object its average translational and rotational diffusion coefficients are defined, respectively, as $D^t = 1/3\text{Tr}(D^{tt})$ and $D^r = 1/3\text{Tr}(D^{rr})$, where the diffusion tensor (eq 1) is evaluated in the molecule-fixed coordinate system with the origin located at the particle's diffusion center.⁵

Most molecular processes that occur in biological systems involve steps that are diffusion-mediated with formation of various specific and nonspecific, either stable or transient complexes. Biological molecules are rarely spherical, and thus, their diffusional behavior can be highly anisotropic. Additionally, intermolecular interactions can also be anisotropic, which may affect the encounters of hydrodynamically isotropic and anisotropic particles differently.

The Brownian dynamics (BD) technique^{1,6–8} allows one to study diffusional transport of molecules in different environments^{9–16} and kinetics of bimolecular association pro-

Received: October 29, 2012

Published: February 18, 2013



cesses.^{17–21} Even though some state-of-the-art applications of BD achieve a high level of sophistication in describing molecules and their interactions,^{13,16,19} most of the BD studies ignore the effects of molecular shapes on Brownian motions and encounters of diffusing objects. Diffusion of molecules is usually assumed to be isotropic, and instead of diffusion tensors, the average translational and rotational diffusion coefficients are used.^{13–21} Studies employing BD algorithms that are based on the full diffusion tensors of molecules are scarce,^{1,12,22,23} and the role of anisotropy in molecular transport and encounters is yet to be clarified.

Recently, Schluttig et al.²³ addressed the issue of hydrodynamic anisotropy by performing rigid-body BD simulations of model particles with no atomic details (i.e., ellipsoids covered with spherical encounter patches). They studied the dependence of encounter rates on the aspect ratio of ellipsoid axes and on the position of spherical encounter patches on ellipsoids' surfaces. The only kind of interaction between the ellipsoids that was accounted for was hard-core repulsion. Schluttig et al. concluded that the encounter rates depend on the aspect ratio of the ellipsoids mostly through steric effects and that the overall influence of anisotropic diffusion on ellipsoid–ellipsoid encounter rates is moderate.²³

Here, we study the association kinetics of a bacterial ribonuclease, barnase, and its natural inhibitor, barstar (Figure 1),²⁴ using the rigid-body BD technique. These two proteins bind fast and with strong affinity. Structural, thermodynamic, and kinetic aspects of barnase–barstar association have been thoroughly studied, both experimentally^{26–33} and theoretically.^{20,21,34–44} Previously, Brownian dynamics simulations were used to estimate absolute values of barnase–barstar association rate constants under different conditions and in the presence of different point mutations.^{20,21} For example, it was shown that BD simulations can predict even very small differences in barnase–barstar association rate constants resulting from point mutations introduced at their binding interface.²¹ BD was also used to address questions regarding optimal association pathways of barnase and barstar, the description of their encounter complex, possible differences of the pathways for dissociation and association, and effects of mutations on their encounter.³⁹

While previous BD studies of the barnase–barstar system neglected hydrodynamic anisotropies of these proteins (this is also true in a more general case, apart from yet another work of Schluttig et al.²² who explored the effect of various coarse-graining strategies for modeling proteins on the rate of their encounter, we are not aware of any BD study on protein–protein association kinetics that would utilize fully anisotropic diffusion tensors of the binding partners). We believe that it is an interesting question, whether (and to what extent) hydrodynamic anisotropy affects the encounter kinetics. We aim to answer this question, using barnase and barstar as a model system. Both barnase and barstar can be considered as typical globular proteins for which the equivalent spheres approach seems to be reasonable and the role of their hydrodynamic anisotropies is not obvious. Moreover, the validity of the rigid-body description of barnase and barstar has been justified in studies of their encounter.³⁶

Even though in our simulations we apply detailed description of proteins and their interactions, our goal is neither to predict the absolute values of association rate constants nor investigate the role of particular interactions in barnase–barstar affinity. The focus of our study is rather the relative magnitude of

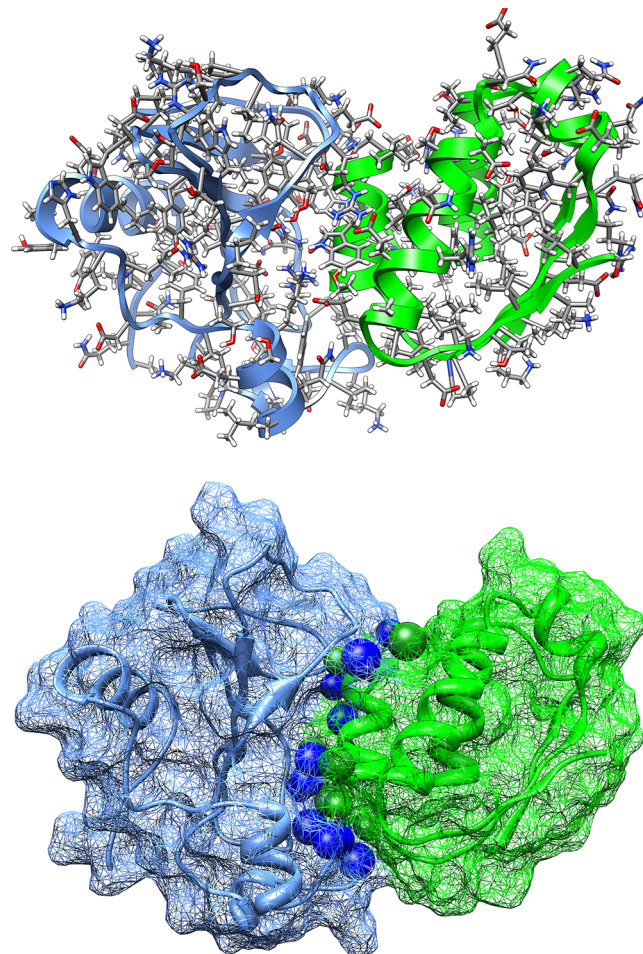


Figure 1. Crystallographic complex between barnase (blue) and barstar (green) (PDB ID 1BGS²⁴). Spheres (bottom) denote atoms of the barnase–barstar binding interface that were used to define the reaction criterion (see text for details). Drawings were done using the UCSF Chimera²⁵ package.

hydrodynamic anisotropy effects on the kinetics of their encounter. We generate BD trajectories of binding partners that are described with either fully anisotropic diffusion tensors or average diffusion coefficients appropriate for hydrodynamically equivalent spheres and then directly compare the association kinetics derived from these simulations. Moreover, we simulate continuous BD trajectories under periodic boundary conditions and thus avoid the simulation protocol⁸ based on the Smoluchowski theory,^{45,46} utilized in previous works.^{20,21,39,43}

2. METHODS

2.1. Brownian Dynamics Simulations. 2.1.1. Rigid-Body Brownian Dynamics Algorithm.

The propagation scheme for an arbitrarily shaped rigid body can be written in the molecule-fixed frame as^{1,8,47}

$$\Delta \vec{x}(\Delta t) = \frac{\Delta t}{k_B T} \mathbf{D} \vec{M} + \vec{R}(\Delta t) \quad (2)$$

where \mathbf{D} is the precomputed (and constant in the simulation) 6×6 diffusion tensor of the molecule evaluated in the molecule-fixed coordinate system with the origin located at the molecule's diffusion center⁵ and axes coinciding with the principal axes of particle's rotations (so that the submatrix \mathbf{D}^r

in eq 1 is diagonal). Δt is the time step, \vec{x} is the vector describing the position of the diffusion center (\vec{r}) and orientation ($\vec{\phi}$) of the molecule, $\vec{x} = (\vec{r}, \vec{\phi})^T$. \vec{M} is a generalized force resulting, for example, from interactions with other molecules or external fields and having two components: the total force (\vec{F}) and the total torque (\vec{T}) referred to the molecule's diffusion center, $\vec{M} = (\vec{F}, \vec{T})^T$. $\vec{R}(\Delta t)$ is a random displacement vector arising from the Brownian noise, with zero mean, and the variance-covariance given with

$$\langle \vec{R}(\Delta t) \vec{R}(\Delta t) \rangle = 2\mathbf{D}\Delta t \quad (3)$$

Random displacements of the particle can be computed via Cholesky decomposition of its diffusion tensor.⁸ Brownian dynamics trajectory of an object in the laboratory frame can be obtained by applying at each BD simulation step properly defined transformations, translations and rotations,¹ between molecule-fixed and laboratory coordinate frames.

2.1.2. Diffusion Tensors. Diffusion tensors of barnase and barstar were computed using the HYDROPRO suite⁴⁸ of Garcia de la Torre assuming water viscosity of 1.0 cP and temperature of 298.15 K using proteins' coordinates from the 1BGS²⁴ PDB structure. The obtained average translational and rotational diffusion coefficients are $1.3 \times 10^{-2} \text{ \AA}^2/\text{ps}$ and $2.5 \times 10^{-5} \text{ 1/ps}$ for barstar and $1.2 \times 10^{-2} \text{ \AA}^2/\text{ps}$ and $1.9 \times 10^{-5} \text{ 1/ps}$ for barnase, respectively. The equivalent radius of a spherical molecule is 18.3 Å in case of barnase and 16.4 Å in case of barstar. As illustrated in Table 1, the shape of the investigated

Table 1. Aspect Ratios D_{ii}^{tt}/D^t and D_{ii}^{rr}/D^r Computed for Rigid-Body Diffusion Tensors of Barnase and Barstar^a

	D_{xx}^{tt}/D^t	D_{yy}^{tt}/D^t	D_{zz}^{tt}/D^t	D_{xx}^{rr}/D^r	D_{yy}^{rr}/D^r	D_{zz}^{rr}/D^r
barnase	0.96	1.05	0.99	0.89	1.15	0.95
barstar	0.99	0.97	1.03	0.97	0.93	1.09

^a $D^t = 1/3 \text{Tr}(D^{tt})$ and $D^r = 1/3 \text{Tr}(D^{rr})$.

proteins deviates from spherical. However, their diffusional behavior only moderately deviates from isotropic with barnase showing larger hydrodynamic anisotropy. Diffusion anisotropy of both proteins is clearly visible when one considers their rotational dynamics (Figure 2). Rotational diffusion of a molecule can be described using the rotational autocorrelation function ($C(t)$); that is, the average of the second Legendre polynomial ($P_2(t)$) of the angle encircled by a molecule-fixed unit vector (\hat{u}) during time t :

$$C(t) = \langle P_2(t) \rangle = \frac{3}{2} \langle \hat{u}(t_o) \hat{u}(t_o + t) \rangle_{t_o} - \frac{1}{2} \quad (4)$$

where the average is taken over an initial state t_o . In case of free diffusion of an arbitrarily shaped rigid body, $\langle P_2(t) \rangle$ is a multieponential function with five components:^{1,49}

$$\langle P_2(t) \rangle = \sum_{i=1}^{i=5} a_i e^{-t/\tau_i} \quad (5)$$

where amplitudes a_i depend on the orientation of the molecule-fixed unit vector and elements D_{ii}^{rr} of the diffusion tensor, whereas relaxation times τ_i depend only on D_{ii}^{rr} .^{1,49} Free diffusion of a spherical molecule is characterized by a monoexponential decay. Figure 2 presents rotational autocorrelation functions obtained from separate BD simulations of barnase and barstar for unit vectors pointing along the principal axes of their rotational diffusion tensors as well as multi-

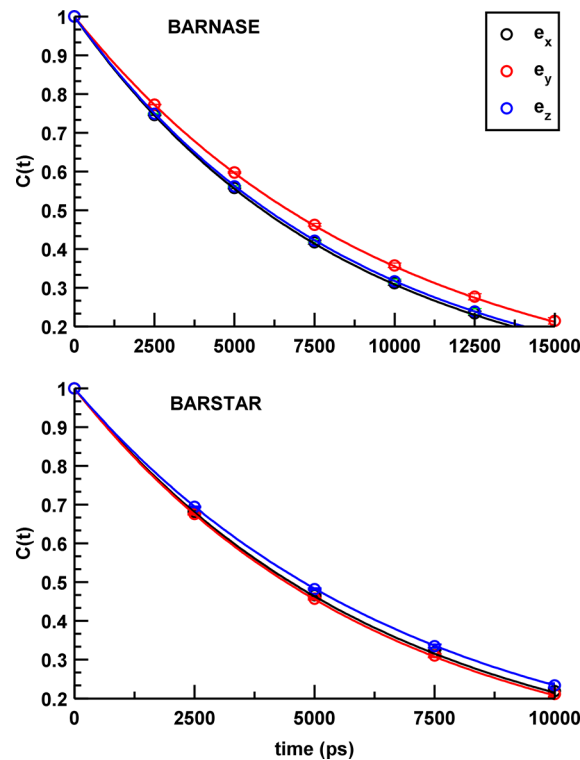


Figure 2. Rotational autocorrelation functions obtained for unit vectors $\hat{e}_x, \hat{e}_y, \hat{e}_z$ pointing along the principal axes of rotational diffusion tensors (D^{rr}) of barnase and barstar, respectively. Empty symbols, average curves obtained for ensembles of independent BD trajectories (standard deviation bars are comparable to the symbols' size). Continuous lines represent theoretical curves;^{1,49} see text for details.

exponential decays computed analytically using expressions given in refs 1 and 49. Observed differences between the autocorrelation functions of $\hat{e}_x, \hat{e}_y, \hat{e}_z$ point to the rotational anisotropy of both proteins.

2.2. Modeling of Intermolecular Interactions. Intermolecular forces between barnase and barstar (eq 2) are computed analytically as derivatives of different potential functions that we describe below.

2.2.1. Protein Models. Atomistically detailed protein models were created based on the X-ray structure of the barnase–barstar complex²⁴ (Figure 1). We used the PROPKA utility⁵⁰ with the CHARMM PARAM22 parameter set⁵¹ to add hydrogens to proteins' heavy atoms as appropriate at pH 8.0.³⁰ Partial charges and radii were assigned using the PDB2PQR tool.⁵² The resulting total protein net charges and number of atoms were +2 e and 1727 (M_{barnase}) for barnase and -6 e and 1432 (M_{barstar}) for barstar, respectively.

2.2.2. Excluded Volume Interactions. Excluded volume interactions were modeled with the standard attractive/repulsive, 6/12 Lennard-Jones terms:

$$\Delta G^{\text{exc}} = 4 \sum_i^{M_{\text{barnase}}} \sum_j^{M_{\text{barstar}}} \sqrt{\varepsilon_i^{\text{LJ}} \varepsilon_j^{\text{LJ}}} \left(\left(\frac{\sigma_i + \sigma_j}{r_{ij}} \right)^{12} - \left(\frac{\sigma_i + \sigma_j}{r_{ij}} \right)^6 \right) \quad (6)$$

with well depths $\varepsilon_i^{\text{LJ}}$ and van der Waals radii σ_i taken directly from the CHARMM PARAM22 parameter set.⁵¹ However, in

our simulations a cutoff of $2^{(1/6)}(\sigma_i + \sigma_j)$ was applied during evaluation of Lennard-Jones (LJ) interactions; thus, effectively, only the short-range repulsion between proteins' atoms was taken into account.

2.2.3. Electrostatic Interactions. Electrostatic interactions between proteins were evaluated based on the effective charges concept.^{53,54}

Effective charges positioned at heavy atoms of the proteins were derived by fitting the electrostatic potential resulting from the Debye–Hückel approximation⁵⁵ to the external molecular potential obtained as a numerical solution of the Poisson–Boltzmann equation.⁵⁶ The electrostatic potentials of barnase and barstar were computed on three-dimensional grids using APBS⁵⁷ based on the linearized Poisson–Boltzmann equation at ionic strength of 200 mM with dielectric constants of proteins and the solvent set to 2 and 78.54, respectively, with protein structures generated by PDB2PQR⁵² and PROPKA.⁵⁰ The effective charges were obtained using the PDC package¹⁷ by solving the system of linear equations:

$$\mathbf{A}\vec{q} = \vec{b} \quad (7)$$

where \vec{q} is the vector of effective charges, the \mathbf{A} matrix is defined as

$$A_{ij} = \int_{\Omega} d^3\vec{r} \frac{\exp(-\kappa|\vec{r} - \vec{r}_i|)}{\epsilon|\vec{r} - \vec{r}_i|} \times \frac{\exp(-\kappa|\vec{r} - \vec{r}_j|)}{\epsilon|\vec{r} - \vec{r}_j|} \quad (8)$$

and the elements of \vec{b} are given by

$$b_i = \int_{\Omega} d^3\vec{r} \frac{\exp(-\kappa|\vec{r} - \vec{r}_i|)}{\epsilon|\vec{r} - \vec{r}_i|} \Phi^{PB}(\vec{r}) \quad (9)$$

In the above equations, Ω denotes the volume outside a molecule where the electrostatic potential is fitted, $\Phi^{PB}(\vec{r})$ is the value of the electrostatic potential at a given point \vec{r} obtained by numerically solving the linearized Poisson–Boltzmann equation, ϵ is the dielectric constant of the solvent, and κ is the inverse of the Debye length, corresponding in the present report to 200 mM of NaCl. The volume Ω was defined as a 5 Å thick skin around a protein with the lower boundary of the skin determined as the van der Waals surface of the protein inflated by 3 Å. The quality of the effective charge fits was judged using the accuracy parameter, χ , defined as

$$\chi = 1 - \frac{\int_{\Omega} d^3\vec{r} \left| \Phi^{PB}(\vec{r}) - \sum q_j \frac{\exp(-\kappa|\vec{r} - \vec{r}_j|)}{\epsilon|\vec{r} - \vec{r}_j|} \right|^2}{\int_{\Omega} d^3\vec{r} |\Phi^{PB}(\vec{r})|^2} \quad (10)$$

In cases of both barnase and barstar, we were able to fit the effective charges with the value of χ above 0.99. Using potential-derived effective charges, the energy of barnase–barstar charge–charge (Coulombic) interactions screened by dissolved ions is described as

$$\Delta G^{\text{charge-charge}} = \sum_i^{N_{\text{barnase}}} \sum_j^{N_{\text{barstar}}} \frac{q_i q_j}{\epsilon} \frac{e^{-\kappa r_{ij}}}{r_{ij}} \quad (11)$$

Additionally, we took into account short-range cavity terms⁵⁸ (or desolvation penalties⁵³) that describe interactions of charges of one of the proteins with the dielectric cavity occupied by the second protein. Considering for example a particular charge of barnase (q_i), one can describe the energy of its interactions with the barstar's dielectric cavity (which is

treated as a conglomerate of low dielectric van der Waals spheres, i.e., atoms) as⁵⁸

$$\Delta G^{\text{cavity}_i-q} = \beta \frac{\epsilon - \epsilon_p}{\epsilon(2\epsilon + \epsilon_p)} \sum_{j=1}^{N_{\text{barstar}}} \frac{(1 + \kappa r_{ij})^2}{r_{ij}^4} \times \exp(-2\kappa r_{ij}) (q_j)^2 (\sigma_i)^3 \quad (12)$$

where σ_j is the van der Waals radius of the j^{th} atom of barstar, ϵ_p is the protein's low dielectric constant, and the empirical scaling factor β is introduced to account for the fact that van der Waals spheres of the protein overlap; its value depends also on the ionic strength.⁵³ Summation runs over all van der Waals spheres (atoms) of barstar (M_{barstar}). Additionally, the i^{th} barnase's dielectric sphere interacts with barstar's effective charges:

$$\Delta G^{\text{cavity}_i-q} = \beta \frac{\epsilon - \epsilon_p}{\epsilon(2\epsilon + \epsilon_p)} \sum_{j=1}^{N_{\text{barstar}}} \frac{(1 + \kappa r_{ij})^2}{r_{ij}^4} \exp(-2\kappa r_{ij}) (q_j)^2 (\sigma_i)^3 \quad (13)$$

where σ_i is the van der Waals radius of the i^{th} barnase's atom and the summation runs over all effective charges of barstar (N_{barstar}).

The value of the scaling factor β in eqs 12 and 13 was set to 0.5 based on the comparison of electrostatic energies of barnase–barstar interactions obtained using the equations given above, with values obtained from Poisson–Boltzmann computations with the APBS package.⁵⁷ Comparison was performed for 30 different random configurations of barnase and barstar (Figure 3) in which proteins' van der Waals surfaces were separated by less than 5 Å. Barnase–barstar configurations were taken from BD simulations that were performed with all interactions between the proteins switched off.

During BD simulations, electrostatic interactions were evaluated within a spherical, atom-based cutoff of 22 Å, a

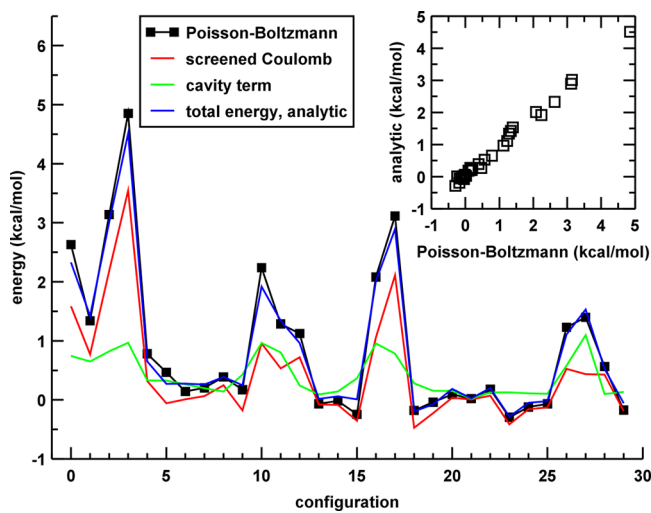


Figure 3. Comparison of electrostatic energies of interactions computed for 30 different barnase–barstar configurations using either the Poisson–Boltzmann solver APBS⁵⁷ or the analytic approach employed in the present work. The correlation coefficient, r , of paired data given in the inset is 0.996; we used Pearson correlation coefficient that for pairs $(X_i, Y_i)_{i=1 \dots n}$ takes the form $r = (\sum_{i=1}^n (X_i - \langle X \rangle)(Y_i - \langle Y \rangle)) / ((\sum_{i=1}^n (X_i - \langle X \rangle)^2)^{1/2}(\sum_{i=1}^n (Y_i - \langle Y \rangle)^2)^{1/2})$.

value that on the one hand is smaller than the half of the primary simulation cell's edge and on the other hand is sufficiently large, considering the effective range of exponentially decaying electrostatic interactions, the Debye length, which at 200 mM is $\sim 6.8 \text{ \AA}$.

2.2.4. Hydrophobic Interactions. Nonpolar (hydrophobic) interactions between proteins were evaluated using the analytical FACTS approach.⁵⁹ In the FACTS model, nonpolar contribution to the free energy of solvation of a molecule is modeled in a rather generic way⁶⁰ in relation to the amount of its surface exposed to the solvent (SASA):

$$\Delta G^{\text{nonpolar}} = \gamma \sum_{i=1}^N \text{SASA}_i \quad (14)$$

where summation runs over all (N) atoms of a protein (or proteins), γ denotes the empirical surface tension parameter,⁶⁰ and atomic SASAs are given with⁵⁹

$$\text{SASA}_i = c_o + \frac{c_1}{1 + e^{-c_2(D_i - c_3)}} \quad (15)$$

$$D_i = \sum_{j \neq i}^N V_j \Theta_{ij} + d_1 \left| \frac{\sum_{j \neq i}^N \frac{V_j}{r_{ij}} \Theta_{ij} \hat{x}_{ij}}{1 + \sum_{j \neq i}^N \frac{V_j}{r_{ij}} \Theta_{ij}} \right| + d_2 \sum_{j \neq i}^N V_j \Theta_{ij} \left| \frac{\sum_{j \neq i}^N \frac{V_j}{r_{ij}} \Theta_{ij} \hat{x}_{ij}}{1 + \sum_{j \neq i}^N \frac{V_j}{r_{ij}} \Theta_{ij}} \right| \quad (16)$$

In the above equations, V_j denotes the van der Waals volume of the j^{th} atom, r_{ij} is the distance between atoms i and j , \hat{x}_{ij} is a unit vector pointing from the i^{th} atom to the neighboring j^{th} atom and Θ_{ij} is a sigmoidal weighting function:

$$\Theta_{ij} = \begin{cases} \left(1 - \left(\frac{r_{ij}}{R_i}\right)^2\right)^2, & \text{if } r_{ij} \leq R_i \\ 0, & \text{if } r_{ij} > R_i \end{cases} \quad (17)$$

where R_i is a predefined radius of a sphere (i.e., cutoff) enclosing the i^{th} atom.

Parameters c_o , c_1 , c_2 , c_3 , d_1 , and d_2 that are derived by fitting to exact values of SASA⁵⁹ were taken from the PARAM22 CHARMM parameter set.⁵¹ For all atoms values of R_i were set to 10 Å, following the original parametrization of the FACTS model.⁵⁹ The surface tension parameter was set to 0.015 kcal/mol·Å⁻² a recommended value from previous molecular dynamics⁵⁹ and protein–ligand docking⁶¹ studies that employed the FACTS model and the PARAM22 parameter set.

2.3. Simulations Setup. All Brownian dynamics simulations were performed using the BD_BOX package.⁶² BD_BOX source code was modified for the purpose of the current study to allow for rigid-body BD simulations of atomistically detailed models of proteins interacting via potentials that are described above. The simulated system consisted of a single barnase and a single barstar molecule. All BD simulations were conducted under periodic boundary conditions with the primary box size of 100 Å × 100 Å × 100 Å. Minimum image convention was applied during evaluation of barnase–barstar interactions. The simulation time step was set to 2 ps, which gives an average displacement in a single BD step

below 1 Å for the studied proteins. This seems an appropriate value if one considers the roughness of protein surfaces resulting from the van der Waals radii of atoms. Solvent viscosity and temperature were set to the same values as for diffusion tensors calculations.

Two kinds of simulations were performed. Both proteins were simulated with either fully anisotropic diffusion tensors or as equivalent spherical particles. For every simulation type we generated 130 BD trajectories of 10 μs each, which gave a total of 1.3 ms. Trajectories were initiated by placing randomly oriented proteins at random positions inside the primary simulation box. Trajectory snapshots were collected every 500 ps for further analysis. We took into account periodic boundary conditions, each trajectory snapshot contained either coordinates of proteins from the primary simulation cell or coordinates of a protein from the primary simulation cell and the closest image of the second protein.

2.4. Encounter Complex. According to the transition state theory, the stereospecific binding of two proteins can be described as a consecutive two-step process.^{34,63} First, proteins approach each other via translational and rotational diffusion and reach a region in configurational space where their separations and orientations are close to those observed in the final complex. Such configurations of proteins constitute the transient complex ensemble. Second, the conformational rearrangement of proteins leads to the stereospecific final (or native) complex, as seen for example in structures obtained from crystallographic experiments. The transient complex ensemble consists of configurations from which the native complex forms instantaneously.^{34,64} The association rate constant can be obtained via calculating the average (over the configurational space of the transient complex ensemble) Boltzmann factor of interactions energies and the basal association rate (i.e., the rate for reaching the transition state in the absence of intermolecular interactions).^{34,64} The basal rate can be determined from BD simulations of noninteracting proteins.³⁴ Combination of BD simulations of noninteracting molecules with the Poisson–Boltzmann electrostatic calculations leads to the association rate constant that is computed as the product of the basal rate and the average Boltzmann factor.³⁴

However, the association kinetics can also be derived by applying the BD technique more directly.⁸ In such applications, some number of independent BD trajectories of the two interacting proteins is generated. The fraction of encounter trajectories, that is, trajectories that end in the formation of an encounter complex that pertains to predefined reaction criteria, is used to estimate the association rate constant. In general, the encounter complex is not the same as the transient state.³⁹ Before reaching the transient complex, proteins first form looser complexes, which are then rearranged into a more orientationally restricted transition state. These somewhat looser complexes form an encounter complex ensemble.

In this report, we do not distinguish between encounter and transient complexes. We will further use the term encounter complex to describe barnase–barstar configurations observed in our BD simulations that satisfy the reaction criterion described below. Resulting complexes range from those close to restrictions imposed by the crystal structure geometry, to others rather loose or even nonspecific.

We applied the following geometric criterion to describe the formation of the barnase–barstar encounter complex. We choose twelve distinct pairs of heavy atoms from the barnase–

barstar interface (Figure 1). The first atom in a given pair belongs to barnase, the second one to barstar. Distances between atoms within these pairs are smaller than 4 Å when measured in the X-ray structure. We define a single parameter to describe the encounter complex of the two proteins, d_X^{BD} , as

$$d_X^{BD} = \sqrt{\frac{1}{N_{\text{pairs}}} \sum_i^{N_{\text{pairs}}} (r_i^{BD} - r_i^X)^2} \quad (18)$$

where N_{pairs} is the number of pairs, r_i^{BD} is the distance within an i^{th} pair measured in simulations and r_i^X is the distance within an i^{th} pair measured in the X-ray barnase–barstar complex. We require d_X^{BD} to be lower than a certain threshold value for an encounter complex formation, and, as kinetic effects of hydrodynamic anisotropy might depend on the particular value selected, we examine several different threshold values.

3. RESULTS AND DISCUSSION

3.1. Characterization of Barnase–Barstar Encounter Complexes.

While it is recognized that the configuration of binding partners in the encounter complex must be close to the one observed in the native complex as without such orientational constraints theoretically predicted association rate constants would be too large,⁶⁴ the definition of the encounter complex is somewhat arbitrary. In the case of barnase and barstar, it was shown in experiments²⁹ that while native-like contacts between charged residues of proteins are present in the transition state, they are weakened, which suggest that they can be mediated by water molecules. In a previous Brownian dynamics study,²¹ the authors applied different definitions of the encounter complex and then chose the one giving the best agreement between association rates determined from BD simulations and experimentally determined values.

However, one can speculate that if some details or properties of the studied system are omitted in BD simulations performed to determine the association rate constants, their lack can be easily compensated by the choice of reaction criteria.

In our work, barnase–barstar configurations were attributed to different encounter complex ensembles based on the value of the reaction criterion, d_X^{BD} . We considered values of d_X^{BD} of 3, 3.5, 4, 5, 6, 7, and 8 Å, resulting in a set of seven encounter complex ensembles for each kind of BD simulations (i.e., simulations employing either isotropic or anisotropic diffusion tensors of proteins).

Regardless their hydrodynamic properties (i.e., whether we use their full diffusion tensors or treat them as hydrodynamically equivalent spheres), barnase and barstar should probe exactly the same relative configurations in the encounter complex during BD simulations, as one does not expect hydrodynamic effects to influence equilibrium properties of the studied system. We evaluated geometries of barnase–barstar encounter configurations using interresidual distances, root-mean-square deviation (RMSD) from the X-ray structure of the barnase–barstar complex and center-to-center distances as measures of the similarity of encounter complex ensembles resulting from each kind of BD simulations.

Figure 4 presents average (computed over encounter complex ensembles) deviations of distances in each of the barnase–barstar interface atom pairs from the corresponding distances measured in the X-ray structure, as a function of d_X^{BD} :

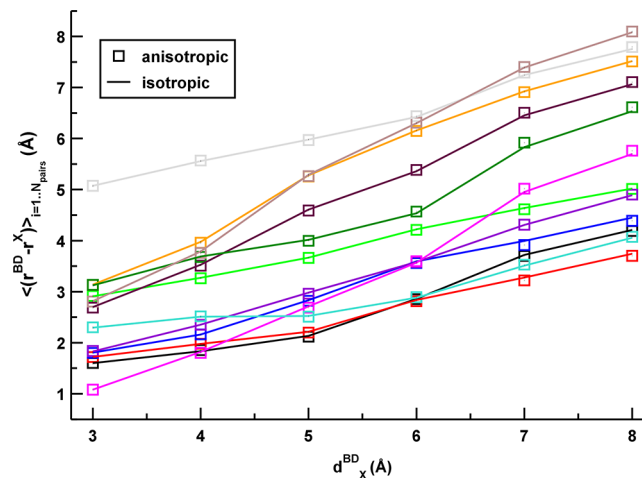


Figure 4. Average (computed over encounter complex ensembles that pertain to the given reaction criterion d_X^{BD}) differences between distances (r_i^{BD}) of atoms in the 12 pairs that are used to define the barnase–barstar encounter complex and the corresponding distances measured in their crystallographic complex (r_i^X), as a function of d_X^{BD} . Different colors are used to denote different (i) atom pairs. Results of BD simulations employing either isotropic or anisotropic diffusion tensors of proteins.

$$\langle r_i^{BD} - r_i^X \rangle_{i=1 \dots N_{\text{pairs}}} = \frac{1}{N_{\text{ensemble}}} \sum_j^{N_{\text{ensemble}}} (r_{i,j}^{BD} - r_{i,j}^X) \quad (19)$$

where i denotes pairs and j runs over barnase–barstar configurations from a given encounter complex ensemble. As expected, plots derived from BD simulations with anisotropic and isotropic diffusion tensors are similar.

A property that can be used to further characterize encounter complexes observed in BD trajectories is the RMSD from the X-ray barnase–barstar configuration. Figure 5 presents distributions of RMSD computed for barnase–barstar config-

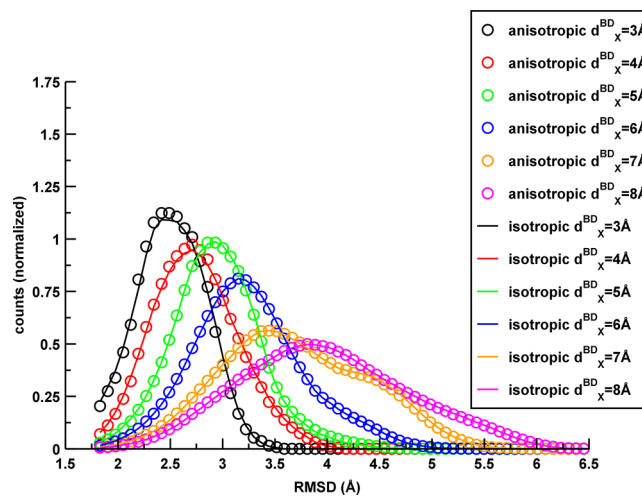


Figure 5. Distributions of heavy atoms root-mean-square deviation (RMSD) between different encounter complexes from BD simulations and the crystallographic barnase–barstar complex. Coordinates of both barnase and barstar were used to superimpose encounter barnase–barstar configurations on their X-ray complex. Results of BD simulations employing either isotropic or anisotropic diffusion tensors of proteins, for different values of the reaction criterion d_X^{BD} , are depicted. Distributions are normalized to unity.

urations that belong to encounter complex ensembles characterized by different values of d_X^{BD} . Distributions obtained for complexes formed in the two types of BD simulations are similar. As can be expected, with an increasing value of d_X^{BD} , computed RMSD values are shifted toward larger values. Moreover, we observe that the less restrictive the reaction criterion (i.e., the larger the value of d_X^{BD}), the wider the corresponding RMSD distribution. The width of the RMSD distribution can be related to the volume of the reactive region. Wider distributions signify smaller orientational restrictions and, thus, the larger volume of the encounter region.

We monitored also center-to-center (by the protein's center, we mean rather its diffusion center than the geometric one) distances in barnase–barstar encounter complexes, the corresponding distance measured in the X-ray barnase–barstar configuration is 22.7 Å. Distributions of these distances from encounter complex ensembles characterized by different values of d_X^{BD} are given in Figure 6. Obtained distributions span the

values of the reaction criterion two sterically allowed but otherwise distinct barnase–barstar configurations are possible. However, for d_X^{BD} values above 5 Å, distributions are no longer bimodal.

Figure 7 presents ensembles of barnase–barstar configurations obtained for different threshold values of d_X^{BD} used for defining the encounter complex. Smaller values of d_X^{BD} result in restricted barnase–barstar configurations in which the relative orientation of proteins is well-defined. Larger values of d_X^{BD} result in complexes in which barnase–barstar interface contacts are disordered as both proteins can substantially rotate relative to their orientations in the native complex. This results in a larger configurational space of the encounter region. Moreover, increased rotations allow for configurations in which proteins' centers of diffusion are closer than in case of configurations restricted by smaller values of d_X^{BD} (Figure 6).

All of the described barnase–barstar encounter complex ensembles were taken into account in the evaluation of association rate constants.

3.2. Barnase–Barstar Association Kinetics. Under the assumption that the association of molecules is irreversible, the rate constant for the bimolecular association process is proportional to the number of particle encounters, observed during a predefined time period. We thus counted the number of barnase–barstar encounters detected for different values of d_X^{BD} in each trajectory from the generated set of 130 BD trajectories. Resulting average values (computed over the set of 130 BD trajectories) are given in Figure 8. Dependencies of the encounter frequency on d_X^{BD} obtained from the two types of BD simulations are overall similar (Figure 8). As expected, smaller values of d_X^{BD} , which correspond to barnase–barstar configurations in the encounter complex that are closer to the configuration observed in the native complex, lead to smaller encounter frequencies and thus smaller association rate constants. However, simulations performed with anisotropic diffusion tensors of barnase and barstar result in more frequent encounters (and thus larger association rate constants, Figure 8) than simulations in which the equivalent spheres approach is employed to describe the binding partners. Moreover, this is observed for the whole range of d_X^{BD} values considered in our study.

Association kinetics can be also described in terms of association (or waiting) times, which are proportional to the inverse of the association rate constant. These are computed as durations that are needed by the two binding partners to reach a configuration characterized by a particular value of d_X^{BD} from the dissociated state. By the dissociated state, we mean any

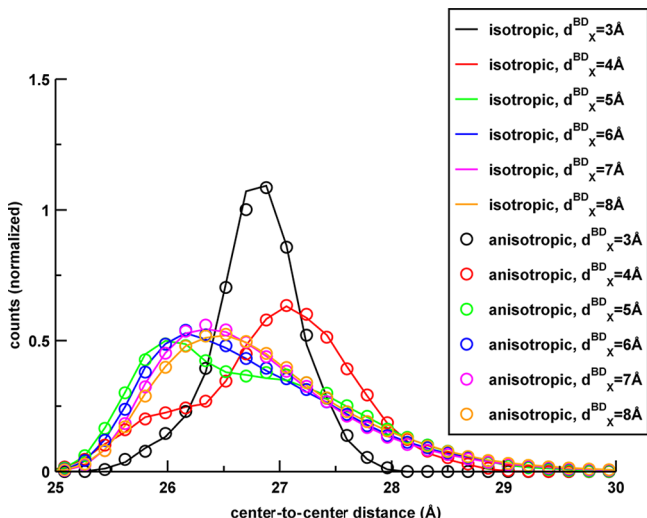


Figure 6. Distributions of barnase–barstar center-to-center distances for different values of the reaction criterion d_X^{BD} . Distributions are normalized to unity.

range between 25 Å and 30 Å. The narrow peak around 27 Å corresponds to d_X^{BD} equal to 3 Å. With an increasing value of d_X^{BD} distributions become wider and asymmetric, with expected values shifted toward slightly shorter center-to-center distances. Moreover, for d_X^{BD} equal to 4 and 5 Å distributions of distances are clearly bimodal, which signifies that, for these particular

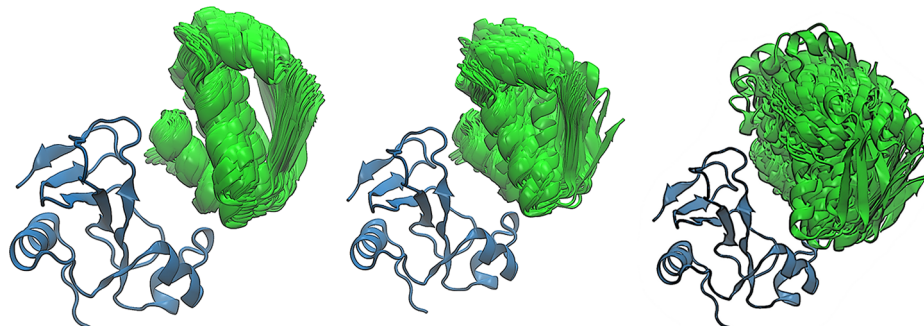


Figure 7. Exemplary encounter complexes of barnase (blue) and barstar (green) from BD simulations that are characterized by d_X^{BD} values of 3 Å (left), 5 Å (center), and 8 Å (right). Protein complexes are superimposed according to coordinates of barnase's atoms for the presentation clarity.

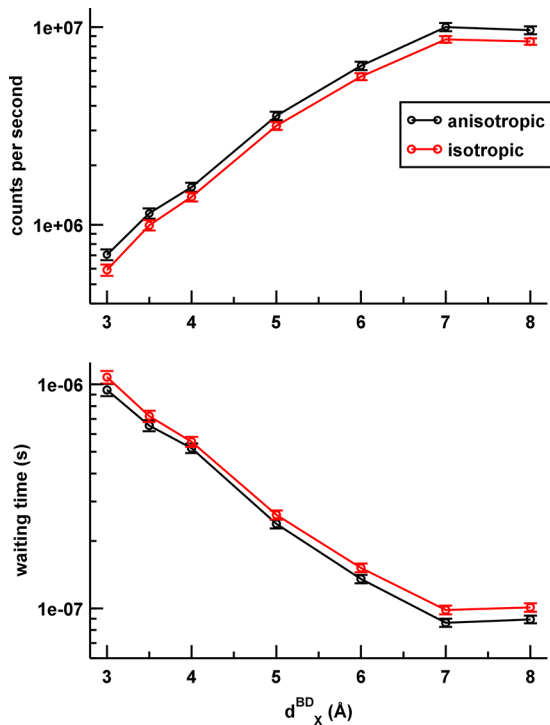


Figure 8. Kinetics of barnase–barstar association. Number of encounters that are registered per second as a function of the reaction criterion d_X^{BD} (top) and association (waiting) times as a function of the reaction criterion (bottom). Error bars represent standard deviations of means. Results of BD simulations employing either isotropic or anisotropic diffusion tensors of proteins are depicted.

barnase–barstar configuration that does not pertain to a given value of d_X^{BD} . Resulting association times, computed as averages over durations extracted from simulated BD trajectories are given in Figure 8. Consistently with results regarding encounter frequencies, waiting times obtained for smaller d_X^{BD} values are longer than those computed for less restrictive encounter definitions. Also, when the equivalent sphere approach is applied to describe barnase and barstar, longer times are required for the association to take place.

Figure 9 presents magnitudes of the diffusion anisotropy effect on the association kinetics evaluated as the relative deviation of the encounter frequencies derived from the two types of Brownian dynamics simulations, $[(\text{counts/second})^{\text{aniso}} / (\text{counts/second})^{\text{iso}}] - 1$, for different values of d_X^{BD} . Hydrodynamic anisotropy effect on the barnase–barstar association kinetics is most pronounced in case of the most restrictive reaction criterion. For d_X^{BD} equal 3 Å, the computed relative deviation is nearly 20% larger when anisotropic diffusion tensors of proteins are employed in BD simulations. Less restrictive definitions of the reaction criterion (i.e., larger values of d_X^{BD}) lead in general to smaller relative magnitudes of the hydrodynamic anisotropy effect, although the changes are neither substantial nor monotonic with increasing d_X^{BD} . It appears from Figure 9 as though the role of the hydrodynamic anisotropy became more visible with the decreasing volume of the encounter complex configurational space (compare with Figure 5). That would signify that the role of the hydrodynamic anisotropy manifests itself primarily in the presence of steric interactions. This conclusion resembles the one that was drawn by Schluttig et al.²³ from a study concerning effect of anisotropy on the encounter rate of ellipsoidal particles covered with

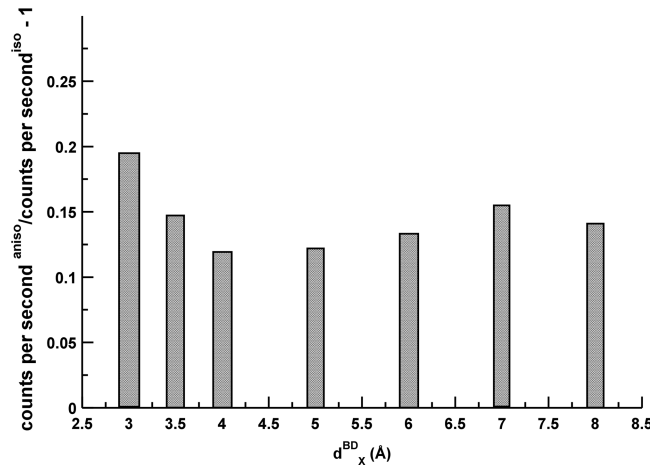


Figure 9. Relative magnitude of the diffusion anisotropy effect on the barnase–barstar association kinetics as a function of the reaction criterion d_X^{BD} .

spherical encounter patches. According to these authors the encounter rate depends on the aspect ratio of ellipsoids primarily through steric effects (i.e., the patch position), while anisotropic diffusion has only a little effect. However, barnase–barstar case differs from the ellipsoids of revolution as the latter are convex bodies with smooth surfaces whereas barnase and barstar contain cavities and their surfaces are rough. The slight variations in the d_X^{BD} dependence of the relative deviation of the encounter frequencies might result from the fact that in the native complex barstar is located in a cavity formed by barnase. Moreover, the association of barnase and barstar is strongly influenced by electrostatic interactions not considered in the study of Schluttig et al.²³ Electrostatic issues will be discussed in the last paragraph of this section.

We analyzed also the role of anisotropic diffusion in case of association toward nonspecific complexes. By nonspecific, we understand barnase–barstar configurations that are not orientationally restricted. We treated the proteins as uniformly reactive spheres and used only their center-to-center distance as the reaction criterion. However, in this case hydrodynamic anisotropy effects on the association kinetics cannot be observed within statistical errors resulting from the applied methodology (Figure 10, left).

Barnase and barstar are complementary from the electrostatic standpoint and electrostatic steering enhances the rate of their encounter above that resulting from simple random search and diffusion. Barnase–barstar association was described as steered by a funnel-shaped free-energy landscape,^{39,44} an analogy adapted from the protein-folding field. Therefore, it is advisable to investigate whether the enhancement of the association rate constant by hydrodynamic anisotropy can be somehow related to the electrostatic steering. For this purpose, we modified the definition of the encounter complex applied in case of nonspecific association by requiring encounters to take place inside a cone whose position and orientation is fixed relative to barnase. The vertex of the cone is defined as the center of barnase, and its axis coincides either with one of the principal axes of barnase's diffusional rotations or with the line connecting centers of proteins in the crystallographic complex (see Supporting Information Figure S1). The angle of the cone is in all cases fixed at $\pi/3$. Encounter is assumed when the diffusion center of barstar enters the interior of the barnase-fixed cone. While the geometry of the encounter complex is

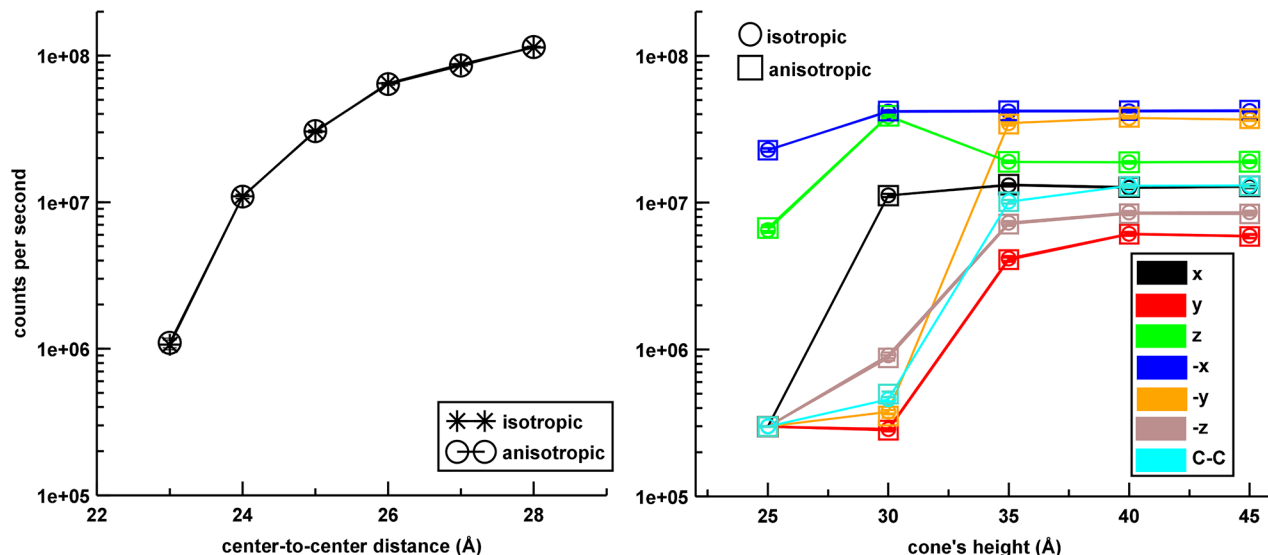


Figure 10. Left: kinetics of nonspecific association of barnase and barstar; number of encounters per second obtained from BD simulations employing either isotropic or anisotropic diffusion tensors of proteins as a function of the center-to-center distance in the encounter complex. Right: number of encounters per second obtained from BD simulations employing either isotropic or anisotropic diffusion tensors of proteins when encounters are assumed to take place inside a barnase-fixed cone; the vertex of the cone is defined as the center of barnase, the axis of the cone coincides either with one of the principal axes of barnase diffusional rotations ($\pm x, \pm y, \pm z$) or with the line connecting centers of proteins in the crystallographic complex (C–C) (see text for details). Error bars that represent standard deviations of means are comparable to the symbols' size.

restricted considering the orientation of the cone relative to barnase no such restrictions are applied to barstar as we do not require barstar to assume a particular orientation inside the cone. Referring to the study by Schlüttig et al.,²³ it corresponds to patching only one of the ellipsoids and leaving the other one having the whole surface equally reactive. Figure 10 (right) shows association kinetics obtained for seven different orientations of the cone where the number of association events is given as a function of the cone's height. The obtained kinetics is different for different orientations of the barnase-fixed cone, which is a consequence first of the electrostatic steering and second of different volumes accessible to barstar in different cones (due to irregularities of protein surfaces and accompanying differences in the volumes that are accessible for barstar). However, even in the regions where barnase–barstar encounter is evidently driven by their electrostatic complementarity,³⁹ hydrodynamic anisotropy does not influence the relative diffusion of proteins, as results obtained with either isotropic or anisotropic diffusion tensors are indistinguishable.

The results described above seem to justify our proposition regarding the relation between anisotropic diffusion effects and configurational restrictions that are present in the reactive region.

3.3. Dissociation from the Encounter Complex. As we have shown, hydrodynamic anisotropy affects association rate constants determined from BD simulations, as far as the specific association of barnase and barstar is considered. However, one may also ask, how does anisotropy of proteins affect the process of their separation after an encounter. To answer this question, we performed the following analysis. Starting from barnase–barstar configurations characterized by a given value of d_x^{BD} (we investigated values of 3, 4, and 5 Å) we evaluated average times needed for the binding partners to reach a somewhat looser (i.e., characterized by a larger value of d_x^{BD}) relative configuration. Resulting escape times are given in Figure 11. We observe that when anisotropic diffusion tensors are employed in BD simulations, escape times are shorter than in

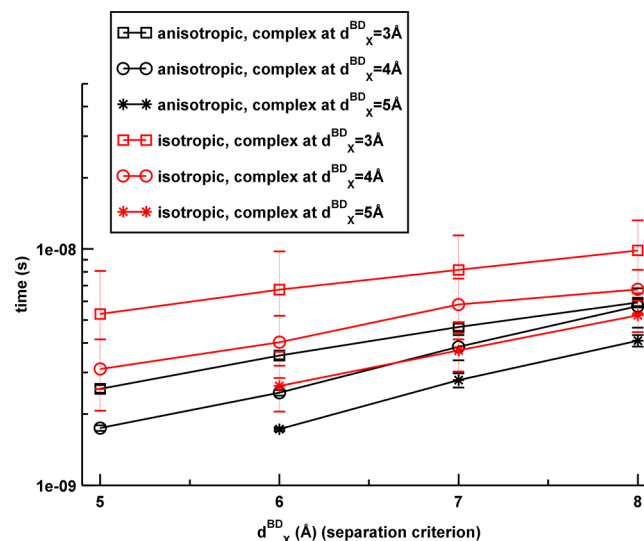


Figure 11. Average escape times from encounter complexes pertaining to different values of the reaction criterion for different definitions of an outer boundary of the encounter complex (separation criterion).

case of BD simulations utilizing isotropic (i.e., equivalent spheres) tensors. Escape of barnase and barstar from the encounter configuration is accelerated by their hydrodynamic anisotropies. This observation is consistent with the described above faster association of proteins toward the encounter complex resulting from their hydrodynamic anisotropy, as the equilibrium constant of the whole process should not be influenced by hydrodynamic anisotropies of binding partners. However, we note that we are not able to provide sensible estimations of dissociation rate constants as the model of proteins used in our simulations lacks short-range interactions and flexibility of proteins' side chains.

4. CONCLUSIONS

We have performed rigid-body BD simulations of atomistic barnase and barstar models and investigated the role of their hydrodynamic anisotropy in the kinetics of their encounter and mutual diffusion. Even though both proteins are only moderately aspherical (see Table 1 and Figure 2) the influence of their anisotropies on the encounter kinetics is clearly visible. We have shown that the relative magnitude of anisotropic diffusion effects can be as large as 20%, when association toward orientationally restricted complexes is considered. However, we were not able to observe anisotropic diffusion effects in the case of nonspecific barnase–barstar encounters. According to our simulations, the effect of hydrodynamic anisotropy manifests itself through excluded volume (or steric) interactions. It appears from our simulations that, at close separations, when described with fully anisotropic diffusion tensors, barnase and barstar more effectively search the configurational space and thus associate faster toward a particular orientationally restricted complex. This also holds true when dissociation from the encounter is considered and we have shown that proteins modeled with fully anisotropic diffusion tensors reach the separated state faster than proteins modeled with isotropic tensors. Taking into account the full 6×6 diffusion tensor of a rigid particle (eq 1), besides anisotropies of its translational and rotational subtensors, one can in general expect some influence of its translational-rotational coupling part. However, in case of barnase and barstar, translational-rotational coupling is negligible, as discussed by Schluttig et al.²² (see also Supporting Information Figure S2 and full diffusion tensors of both proteins that are given in the Supporting Information), and all effects on the encounter rate observed in our simulations result exclusively from anisotropies of the proteins translation and rotation subtensors and the mutual direct interactions between the proteins.

Notably, the relative differences between the rates obtained in some BD simulations for barnase and barstar mutants are of similar magnitude,²¹ as the changes in kinetics resulting from anisotropic description of proteins described here.

The focus of our study is the association of barnase and barstar; certainly, we are not able to generalize regarding the role of hydrodynamic anisotropy in protein–protein encounters. However, one can speculate that the role of anisotropy might be far more important in case of diverse multicomponent reaction systems or in physiologically concentrated solutions where the diffusion of objects is restricted. We have been currently investigating this issue. Another factor that may possibly enlarge the anisotropy effects, which we have not taken into account here, are hydrodynamic interactions between associating molecules. It has been shown that hydrodynamic interactions between associating species influence the encounter rates derived from BD simulations.^{43,65} One may also expect that the hydrodynamic coupling between diffusing molecules will influence their encounters differently for isotropic and anisotropic objects. Unfortunately, there is currently no theory that would allow one to evaluate efficiently hydrodynamic correlations between arbitrarily shaped rigid proteins in BD simulations.

■ ASSOCIATED CONTENT

S Supporting Information

Figure showing orientations of the principal axes of the rotational diffusion tensor of barnase. Complete diffusion tensors of barnase and barstar and an analysis of the magnitude of their $D^{tr/tr}$ blocks. This information is available free of charge via the Internet at <http://pubs.acs.org>

■ AUTHOR INFORMATION

Corresponding Author

*Phone: +48 22 5540 818. Fax: +48 22 5540 801. E-mail: mdlugosz@cent.uw.edu.pl

Notes

The authors declare no competing financial interest.

■ ACKNOWLEDGMENTS

The authors acknowledge support from National Science Centre (N N519 646640). This research was supported in part by PL-Grid Infrastructure (ACK Cyfronet AGH). J.M.A. is supported by the University of Warsaw, Faculty of Physics. We are grateful to Paweł Zieliński for modifications of the BD_BOX source code.

■ REFERENCES

- (1) Fernandes, M. X.; de la Torre, J. G. *Biophys. J.* **2002**, *83*, 3039–3048.
- (2) Carrasco, B.; de la Torre, J. G. *Biophys. J.* **1999**, *76*, 3044–3057.
- (3) de la Torre, J. G.; Bernadó, P.; Pons, M. *Methods Enzymol.* **2005**, *394*, 419–430.
- (4) de la Torre, J. G.; Ortega, A.; Amorós, D.; Schmidt, R. R.; Cifre, J. G. H. *Macromol. Biosci.* **2010**, *10*, 721–730.
- (5) Harvey, S.; de la Torre, J. *Macromolecules* **1980**, *13*, 960–964.
- (6) Deutsch, J. M.; Oppenheim, I. *J. Chem. Phys.* **1971**, *54*, 3547–3556.
- (7) Dickinson, E.; Allison, S. A.; McCammon, J. A. *J. Chem. Soc. Faraday Trans. 2* **1985**, *81*, 591–601.
- (8) Ermak, D. L.; J. A. McCammon, J. A. *J. Chem. Phys.* **1978**, *69*, 1352–1360.
- (9) Ridgway, D.; Broderick, G.; Lopez-Campistrous, A.; M. Ru'aini, M.; Winter, P.; Hamilton, M.; Boulanger, P.; Kovalenko, A.; Ellison, M. J. *Biophys. J.* **2008**, *94*, 3748–3759.
- (10) Wieczorek, G.; Zielenkiewicz, P. *Biophys. J.* **2008**, *95*, 5030–5036.
- (11) Ermakova, E.; Krushelnitsky, A. G.; Fedotov, V. D. *Mol. Phys.* **2009**, *100*, 2849–2855.
- (12) Ando, T.; Skolnick, J. *Proc. Natl. Acad. Sci. U.S.A.* **2010**, *107*, 18457–18462.
- (13) McGuffee, S. R.; Elcock, A. H. *PLoS Comput. Biol.* **2010**, *6*, 1–18.
- (14) Elcock, A. H. *Proc. Natl. Acad. Sci. U.S.A.* **2003**, *100*, 2340–2344.
- (15) McGuffee, S. R.; Elcock, A. H. *J. Am. Chem. Soc.* **2006**, *128*, 12098–12110.
- (16) Mereghetti, P.; Gabdoulline, R. R.; Wade, R. C. *Biophys. J.* **2010**, *99*, 782–791.
- (17) Dlugosz, M.; Huber, G. A.; McCammon, J. A.; Trylska, J. *Biopolymers* **2011**, *95*, 616–627.
- (18) Gabdoulline, R. R.; Wade, R. C. *Methods* **1998**, *14*, 329–341.
- (19) Gabdoulline, R. R.; Wade, R. C. *J. Am. Chem. Soc.* **2009**, *131*, 9230–9238.
- (20) Wang, T.; Tomic, S.; Gabdoulline, R.; Wade, R. *Biophys. J.* **2004**, *87*, 1618–1630.
- (21) Gabdoulline, R. R.; Wade, R. C. *Biophys. J.* **1997**, *72*, 1917–1929.
- (22) Schluttig, J.; Almanova, D.; Helms, V.; Schwartz, U. S. *J. Chem. Phys.* **2008**, *129*, 155106.

- (23) Schluttig, J.; Korn, C. B.; Schwarz, U. S. *Phys. Rev. E*. **2010**, *81*, 030902(R).
- (24) Guillet, V.; Lapthorn, A.; Hartley, R.; Mauguen, Y. *Structure* **1993**, *1*, 165–176.
- (25) Pettersen, E. F.; Goddard, T. D.; Huang, C. C.; Couch, G. S.; Greenblatt, D. M.; Meng, E. C.; Ferrin, T. E. *J. Comput. Chem.* **2004**, *25*, 1608–1612.
- (26) Makarov, A.; Protasevich, I.; Lobachov, V.; Kirpichnikov, M.; Yakovlev, G.; Gillib, R.; Briandb, C.; Hartley, R. *FEBS Lett.* **1994**, *354*, 251–254.
- (27) Frisch, C.; Fersht, A.; Schreiber, G. *J. Mol. Biol.* **2001**, *308*, 69–77.
- (28) Zhuravleva, A.; Korzhnev, D.; Nolde, S.; Kay, L.; Arseniev, A.; Billeter, M.; Orekhov, V. *J. Mol. Biol.* **2007**, *367*, 1079–1092.
- (29) Schreiber, G.; Fersht, A. *J. Mol. Biol.* **1995**, *248*, 478–486.
- (30) Schreiber, G. A.; Ferscht, A. R. *Biochemistry* **1993**, *32*, 5145–5150.
- (31) Schreiber, G.; Frisch, C.; Fersht, A. *J. Mol. Biol.* **1997**, *270*, 111–122.
- (32) Mitkevicha, V.; Schulgab, A.; Ermolyukb, Y.; Lobachov, V.; Chekhov, V.; Yakovlev, G.; Hartley, R.; Pace, C.; Kirpichnikov, M.; Makarov, A. *Biophys. Chem.* **2003**, *105*, 383–390.
- (33) Sekatskii, S.; Favre, M.; Dietler, G.; Mikhailov, A.; Klinov, D.; Lukash, S.; Deyev, S. *J. Mol. Recognit.* **2010**, *23*, 583–588.
- (34) Vijayakumar, M.; Wong, K.-Y.; Schreiber, G.; Fersht, A. R.; Szabo, A.; Zhou, H.-X. *J. Mol. Biol.* **1998**, *278*, 1015–1024.
- (35) Selzer, T.; Schreiber, G. *J. Mol. Biol.* **1999**, *287*, 409–419.
- (36) Kieslich, C.; Gorham, R., Jr.; Morikis, D. *J. Non-Cryst. Solids* **2011**, *357*, 707–716.
- (37) Ababou, A.; van der Vaart, A.; Gogone, V.; Merz, K., Jr. *Biophys. Chem.* **2007**, *125*, 221–236.
- (38) Hoefling, M.; Gottschalk, K. *J. Struct. Biol.* **2010**, *171*, 52–63.
- (39) Spaar, A.; Dammer, C.; Gabdoulline, R. R.; Wade, R.; Helms, V. *Biophys. J.* **2006**, *90*, 1913–1924.
- (40) Ji, C.; Zhang, J. *J. Comput. Chem.* **2012**, *33*, 1416–1420.
- (41) Lee, L.-P.; Tidor, B. *Protein Sci.* **2001**, *10*, 362–377.
- (42) Camacho, C.; Weng, Z.; Vajda, S.; DeLisi, C. *Biophys. J.* **1999**, *76*, 1166–1178.
- (43) Frembgen-Kesner, T.; Elcock, A. *Biophys. J.* **2010**, *99*, L75–L77.
- (44) Wang, L.; Siu, S. W. I.; Helms, V. *Biopolymers* **2010**, *93*, 977–985.
- (45) Smoluchowski, M. V. *Phys. Z.* **1916**, *17* (557–571), 585–599.
- (46) Smoluchowski, M. V. *Z. Phys. Chem.* **1917**, *92*, 129–168.
- (47) Allison, S. *Macromolecules* **1991**, *24*, 530–536.
- (48) de la Torre, J. G.; Huertas, M. L.; Carrasco, B. *Biophys. J.* **2000**, *78*, 719–730.
- (49) de la Torre, G.; Harding, S. E.; Carrasco, B. *Eur. Biophys. J.* **1999**, *28*, 119–132.
- (50) Li, H.; Robertson, A. D.; Jensen, J. H. *Proteins* **2005**, *61*, 704–721.
- (51) MacKerell, A. D., Jr.; Bashford, D.; Bellott, M.; Dunbrack, R., Jr.; Evanseck, J.; Field, M.; Fischer, S.; Gao, J.; Guo, H.; Ha, S.; Joseph-McCarthy, D.; Kuchnir, L.; Kuczera, K.; Lau, F.; Mattos, C.; et al. *J. Phys. Chem. B* **1998**, *102*, 3586–3616.
- (52) Dolinsky, T. J.; Czodrowski, P.; Li, H.; Nielsen, J. E.; Jensen, J. H.; Klebe, G.; Baker, N. A. *Nucleic Acids Res.* **2007**, *35*, W522–W525.
- (53) Gabdoulline, R. R.; Wade, R. C. *J. Phys. Chem.* **1996**, *100*, 3868–3878.
- (54) Beard, D. A.; Schlick, T. *Biopolymers* **2001**, *58*, 106–115.
- (55) Bell, G. M.; Levine, S.; McCartney, L. N. *J. Colloid Interface Sci.* **1970**, *33*, 335–359.
- (56) Gilson, M. K.; Honig, B. *Proteins: Struct., Func., Genet.* **1988**, *3*, 32–52.
- (57) Baker, N. A.; Sept, J. D.; Joseph, S.; Holst, M. J.; McCammon, J. A. *Proc. Natl. Acad. Sci. U.S.A.* **2001**, *98*, 10037–10041.
- (58) Li, X.; Levin, Y.; Fisher, M. *Europhys. Lett.* **1994**, *26*, 683–688.
- (59) Haberthür, U.; Caflisch, A. *J. Comput. Chem.* **2008**, *29*, 701–715.
- (60) Roux, B.; Simonson, T. *Biophys. Chem.* **1999**, *78*, 1–20.
- (61) Zoete, V.; Grosdidier, A.; Cuendet, M.; Michelin, O. *J. Mol. Recognit.* **2010**, *23*, 457–461.
- (62) Dlugosz, M.; Zieliński, P.; Trylska, J. *J. Comput. Chem.* **2011**, *32*, 2734–2744.
- (63) Shoup, D.; Szabo, A. *Biophys. J.* **1982**, *40*, 33–39.
- (64) Alsallaq, R.; Zhou, H. *Proteins* **2008**, *71*, 320–335.
- (65) Antosiewicz, J.; McCammon, J. A. *Biophys. J.* **1995**, *69*, 57–65.